JOURNAL OF THE ROYAL SOCIETY Interface

FirstCite® e-publishing

*J. R. Soc. Interface*
doi:10.1098/rsif.2010.0702
*Published online*

# A highly distributed Bragg stack with unique geometry provides effective camouflage for Loliginid squid eyes

**Amanda L. Holt[1,†], Alison M. Sweeney[1,*,†], Sönke Johnsen[2] and Daniel E. Morse[1]**

[1]*Molecular, Cellular and Developmental Biology, and Institute for Collaborative Biotechnology, University of California, Santa Barbara, CA 93106-5100, USA*
[2]*Department of Biology, Duke University, Durham, NC 27708, USA*

Cephalopods possess a sophisticated array of mechanisms to achieve camouflage in dynamic underwater environments. While active mechanisms such as chromatophore patterning and body posturing are well known, passive mechanisms such as manipulating light with highly evolved reflectors may also play an important role. To explore the contribution of passive mechanisms to cephalopod camouflage, we investigated the optical and biochemical properties of the silver layer covering the eye of the California fishery squid, *Loligo opalescens*. We discovered a novel nested-spindle geometry whose correlated structure effectively emulates a randomly distributed Bragg reflector (DBR), with a range of spatial frequencies resulting in broadband visible reflectance, making it a nearly ideal passive camouflage material for the depth at which these animals live. We used the transfer-matrix method of optical modelling to investigate specular reflection from the spindle structures, demonstrating that a DBR with widely distributed thickness variations of high refractive index elements is sufficient to yield broadband reflectance over visible wavelengths, and that unlike DBRs with one or a few spatial frequencies, this broadband reflectance occurs from a wide range of viewing angles. The spindle shape of the cells may facilitate self-assembly of a random DBR to achieve smooth spatial distributions in refractive indices. This design lends itself to technological imitation to achieve a DBR with wide range of smoothly varying layer thicknesses in a facile, inexpensive manner.

**Keywords: Bragg reflector; reflectin; self-assembly; transfer-matrix; camouflage; squid**

## 1. INTRODUCTION

Using transparency and reflection, animals residing in the ocean's featureless midwater environment can make themselves nearly invisible to potential predators. Different optical strategies are found in different types of tissues; while muscles and connective tissue can be made transparent for highly absorbing body parts such as eyes and guts, reflection is a ubiquitous strategy for camouflage. Since the pelagic light field in regions of the ocean with asymptotic light regimes is roughly cylindrical, radiance matching can be an effective strategy for reflective camouflage; if an animal can perfectly reflect, with the same intensity and spectral composition, light radiating from behind a viewer, this reflectance will also match the light radiating from behind the animal, and the animal will remain inconspicuous on its background. Since the reflectors involved in this camouflage strategy are also required to be thin (they must be thinner than the organism's skin), dielectric mirrors provide a highly effective, energy-efficient strategy for camouflage in open water.

In general, mirrors made of either a smooth metal surface or with alternating layers of contrasting refractive index [distributed Bragg reflectors (DBRs)] can be used for specular reflection of broad or narrow ranges of frequency. In the visible electromagnetic spectrum, metallic mirrors typically exhibit broadband reflectance, while Bragg mirrors typically reflect more restricted bands (called the 'bandgap') that span a narrower region of the spectrum. Bandgaps of periodic DBRs with a narrow range of spatial frequencies can be broadened by increasing the refractive index contrast, but the contrast required to span the visible region is greater than that found in biological materials. In the case of biological materials, broadband reflectance from a DBR can be achieved by increasing the range of layer thicknesses within the stack along the direction of incoming light.

There are several structural strategies for accomplishing an increased spatial distribution of layers in a DBR: (i) a random distribution of layer thicknesses

*Author for correspondence (sweeney@lifesci.ucsb.edu).
†These authors contributed equally to this study.

Electronic supplementary material is available at http://dx.doi.org/10.1098/rsif.2010.0702 or via http://rsif.royalsocietypublishing.org.

*Received* 10 December 2010
*Accepted* 24 January 2011

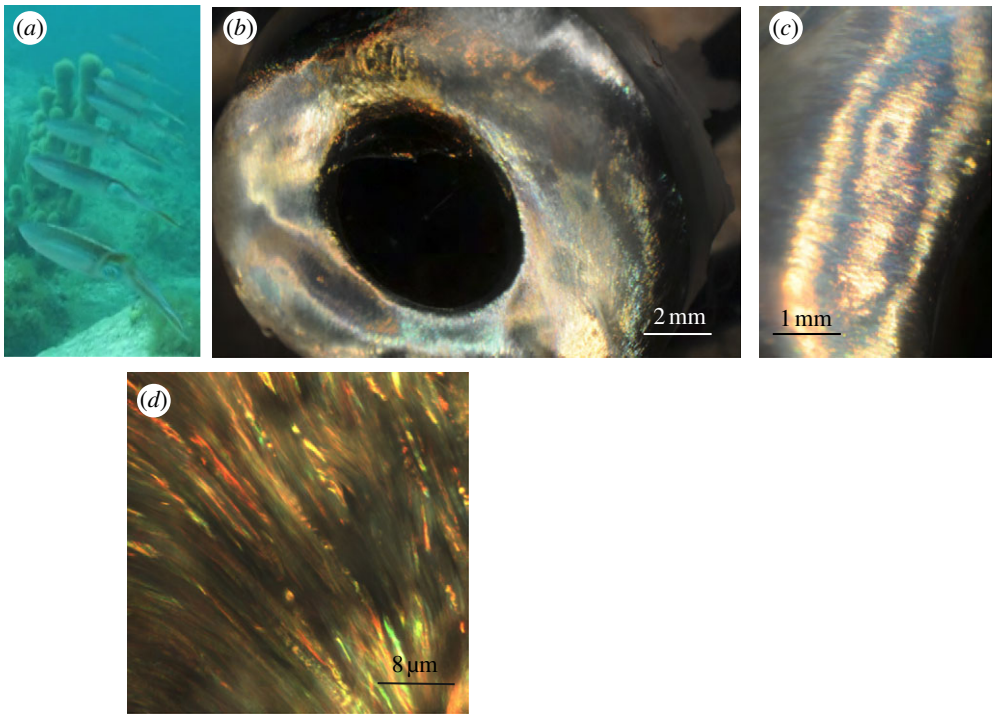


Figure 1. (*a*) Loliginind squid schooling under ambient lighting in shallow water showing effective camouflage of the large eye structure. (*b*) Photograph of squid eye showing relationship of silver tissue to other eye structures. (*c*) Magnification of 10× of the eye covering showing texture. (*d*) Dark-field reflectance micrograph showing complex structure of the silver layer reflectance, and laminated spindle cells (*L. opalescens*).

[1]; (ii) an ordered distribution of layer thicknesses (a.k.a. 'chirped'); and (iii) a stack of several single spatial frequency DBRs with narrow bandgaps on top of each other resulting in broadband reflection. Nature has mastered several of these optical structures, for example, chaotically spaced silver reflectors in fish [2], chirped bronze-coloured beetle reflectors [3] and silver butterfly wings that use a colour-additive technique [4]. Here, we describe for a novel optical and structural design for a broadband DBR, found in the silvery covering of squid eyes from the family Loliginidae. This silvery covering consists of packed spindle-shaped cells that achieve broadband visible reflectance by creating a large range of layer thicknesses. The silvery covering of the squid eye apparently matches the background radiance of the water column in which the animal is immersed, thereby hiding the retina by creating the illusion of transparency (figure 1).

The broadband reflectors found in the squid eye tissue are densely packed protein-rich spindle-shaped cells with a refractive index of 1.56 [5] surrounded by cytoplasm with a refractive index of approximately 1.33 [6]. The optical structure of this eye covering is intriguingly different from the reported broadband reflecting structures in fish scales, because the average size and variation of both the high- and low-refractive index regions is up to ten times that described in fish scales, while the difference between high- and low-refractive index is 0.23 rather than 0.5 (guanine, found in fish scales, has a refractive index of 1.83) [2]. Therefore, in addition to guanine-based reflectors, evolution has also fostered the formation of proteinaceous (therefore polymer-based) broadband dielectric reflectors with layers made from entire cells as a form of midwater camouflage.

Because periodic or randomized DBRs are specular reflectors, the incident angle of incoming light is equal to the angle at which light is reflected and both the wavelength and the intensity of reflection vary with angle. However, the shape of the reflectance spectrum of the squid eye is independent of incident angle, while the reflected radiance drops slightly at oblique angles. Random DBRs are frequently examined and used as optical components such as filters, microcavities and waveguides, where broadband optical reflection can be advantageous [7], and understanding this kind of biological system could lead to inspiration for spindle-based three-dimensional angle-independent broadband reflectors (e.g. ellipsoidal three-dimensional photonic crystals [8]).

For this optical design to behave like a DBR, a large contrast in refractive index must exist between the cells and the cytoplasm, which in the case of the non-crystalline reflectors in squids, probably requires proteins specifically evolved for optical function. In the tissue covering, the Loliginid squid eye, this structure achieves refractive index contrast using cells that are densely and homogeneously filled with protein for high refractive index, and an expanded extracellular space containing mostly water for low refractive index. We also investigated the biochemical composition of the high-refractive index component of this novel reflector, and found a stereotyped protein composition, reminiscent of that found in lens cells that also serve an optical function [9,10]. In this case, the handful of highly expressed proteins in the tissue is comprised of reflectin homologues in addition to a novel, highly

hydrophobic protein with implications for the self-assembly mechanisms responsible for forming these DBR structures.

In the context of their environment, squid eyes seem particularly inconspicuous given the high contrast nature of the large, dark pupil in the centre of a silvery eyeball structure (figure 1*a*). In this report, we describe the biological, cellular and optical properties of the tissue covering the eyes of Loliginid squid (figure 1*b*), which serves as a static reflector for optical camouflage. We focus on the manner in which the long, spindle-shaped cells in the eye tissue (figure 1*c–e*) are arranged to achieve broadband specular reflectance and investigate the details of the reflectance of this tissue in the context of the radiance fields in which it evolved.

## 2. MATERIAL AND METHODS

### 2.1. Animal collection and dissection

Specimens of *Loligo opalescens* were collected by dip-netting near commercial light boats (specialized working vessels used to attract squid) near Ventura, CA on several occasions throughout 2008 and 2009, and transporting to UCSB in aerated coolers. They were maintained in large concrete tanks with running ambient sea water overnight before use. The animals were decapitated and the eyes were dissected from the head. For optical measurements, the intact silver layer was used. Otherwise, the silver layer covering the eye was removed with forceps and frozen in RNAlater (Ambion), or prepared for atomic force microscopy (AFM) and transmission electron microscopy (TEM) experiments described below.

### 2.2. Light microscopy

Cells from the silver tissue were dispersed onto a slide in sea water and photographed under Kohler, phase and differential interference contrast (DIC) illumination. Silver tissue was fixed in 4 per cent paraformaldehyde and 1 per cent of the nucleic acid stain 4′,6-diamidino-2-phenylindole (DAPI) at 4°C overnight. Tissue was then visualized via fluorescence using a mercury lamp light source and a filter cube allowing 365 nm excitation and viewing emission at 420 nm (filter set 02, Zeiss).

### 2.3. Reflectance spectroscopy

Reflectance measurements of the tissue were conducted using a USB2000 spectrometer and SpectraSuite operating software (Ocean Optics, Dunedin, FL, USA). Using fine forceps, the entire eye's covering of silver tissue was delicately removed intact from the eye in a single circular piece. For specular angle-dependence measurements, the peeled silver tissue was laid intact onto a glass slide that was then mounted over the aperture of a goniometer designed for fibre-optic spectrometers (Ocean Optics RSS-VA) (figure 2). Tissue was kept damp with sea water throughout measurements to maintain relative refractive indices, as the optical structure is destroyed with dehydration. Standing water on the surface of the tissue was eliminated immediately prior to the measurement, such

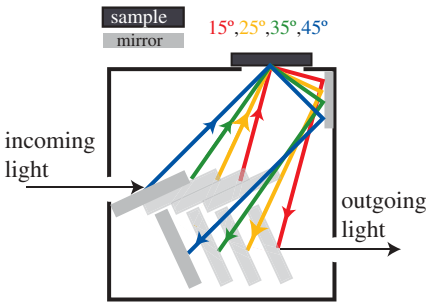


Figure 2. Schematic showing the geometry of the instrument used for changing the angle of incidence and angle of measurement on the silver tissue.

that any possible specular reflections from a damp surface were significantly reduced. Using a circular beam centred on a quadrant of the silver tissue prep (to avoid the central pupil hole), a single measurement represents a spatial average of the entire eye tissue. We used Spectralon, a diffuse reflectance standard, as the silver tissue has a significant component of diffuse reflectance. With three ports, one for incoming light, one for outgoing light and one to view the sample, measurements with this instrument are taken by simultaneously adjusting the angle of incidence and angle of observation from 15° to 45°. The standard was placed against the sample port of the goniometer instrument (Ocean Optics) for measurement when incident light was at 25° and this measurement used for standardizing measurements at all other angles. Given the underlying optical structure we observed, scattered light from the tissue has both specular and diffuse components and our measurements account only for the specular component. Several eye samples were measured and owing to the nature of the tissue preparation, absolute reflectances varied by 10–20% from one sample to the other. As the relative differences in spectra that resulted from changing the angle of incidence remained constant across all samples (data not shown), a single representative set of spectra is presented to illustrate the important features described.

### 2.4. Transmission electron microscopy

For TEM, 3 × 3 mm squares of the silver eye tissue layer were fixed in 2 per cent glutaraldehyde in sea water overnight at 4°C, desalted via graded dilutions of phosphate-buffered saline and then post-fixed in 2 per cent $OsO_4$ for 15 min at room temperature. Samples were then dehydrated through a graded series of ethanol and acetone, and embedded in low-viscosity Spurr's resin according to the manufacturer's instructions (Electron Microscopy Sciences, Hatfield, PA, USA). Ultrathin samples (*ca* 100 nm) were cut on a Leica microtome onto copper grids and imaged on a JEOL electron microscope. The orientation of the section to the knife was such that the face plane of the section was perpendicular to the long axis of the cells, to obtain the photonic geometry experienced by a photon with normal incidence to the external surface of the eye. An interpretation of this three-dimensional

reconstruction is shown as a video in electronic supplementary material.

### 2.5. Atomic force microscopy

For AFM of the separated cells, fresh tissue was gently dispersed with forceps in a drop of sea water placed on a poly-L-lysine-coated glass slide. This process causes thousands of transparent cells to delaminate and settle over the slide. The cells were allowed to adhere to the poly-L-lysine for 1 h, and then washed vigorously with sea water from a laboratory wash bottle to remove any unadhered cells. Tapping-mode AFM in sea water using an Asylum MFP-3D-BIO AFM with a silicon nitride cantilever having a spring constant of 0.08 N $m^{-1}$ was used to image the adhered cells.

### 2.6. Electrophoresis, western blotting and amino acid analysis

One-dimensional sodium dodecyl sulphate–polyacrylamide gel electrophoresis (one-dimensional SDS–PAGE in the presence of detergent) was performed under protein-denaturing conditions on silver tissue extracted and clarified in Laemmli buffer with 2 per cent β-mercaptoethanol. Samples were loaded onto a 10–20% gradient polyacrylamide gel (Invitrogen) in tris-glycine buffer. The resulting electrophorogram was electroblotted onto a polyvinylidene fluoride (PVDF) membrane in Towbin transfer buffer and blocked with 3 per cent bovine serum albumen in phosphate buffered saline + tween (PBST). The blot was then incubated with the primary antibody to *L. opalescens* dermal reflectin 1A diluted 1 : 1000 in blocking solution overnight at 4°C [11]. The blot was washed in PBST three times and then incubated with horseradish peroxidase-conjugated goat-antirabbit secondary antibody in blocking solution in a 1 : 20 000 dilution for 1 h. The membrane was washed in PBST and developed with luminol solution (Pierce) and exposed to film [11].

Amino acid composition of these proteins was then determined with a Beckman autoanalyser. A one-dimensional SDS–PAGE gel electrophoresis, prepared as above, was electroblotted onto PVDF, which was then stained with Coomassie blue to visualize protein bands. Bands of interest and an unstained negative control region of the membrane were excised with new razor blades from the membrane. Membrane fragments were subjected to complete acid hydrolysis under vacuum and loaded in the autoanalyser according to the manufacturer's instructions. Because there was glycine in our electrophoresis buffer, all glycine values were corrected for the glycine content of a blank membrane control sample.

### 2.7. Optical modelling

The modelling program was generated in Matlab (MathWorks, Natick, MA, USA) and uses the general transfer-matrix method to calculate specular reflectance from a one-dimensional stack of alternating high- and low-refractive index elements [12] (hereafter called 'layers'). Transfer-matrix modelling is a simple and elegant technique that provides an exact electromagnetic solution using Fresnel coefficients for specular transmission and reflection of light from parallel stacks of infinite planes. We assumed each layer to be homogeneous and non-absorbing with respect to optical density and the incoming light to be unpolarized. To account for partial incoherence in the specular reflections caused by small inhomogeneities on the surface of each layer, we adjusted the phase components of the Fresnel coefficients with terms representing Gaussian-distributed fluctuations about a 'roughness factor' $Z$ [13,14]. These adjustments are typically used to reduce either undetectable or suppressed Fabry-Perot oscillations caused by multiple coherent reflections within layers with thicknesses greater than the incident wavelength. Models similar to this have been used in other work such as those studying chaotic fish scale reflectors and ordered Bragg reflections in cephalopod skin [2,15]. Using the transfer-matrix model, we can gain insights into how the distribution of layer thicknesses in the silver reflector stack affects the specular reflectance at any incident angle.

Model input parameters were number of layers, distribution of layer thicknesses with alternating high- and low-refractive index within the stack, refractive indices of these layers, angle of incidence and the roughness factor $Z$. The number of layers was chosen such that, given a particular distribution with a defined mean and variance, the total thickness of the stack was 550 μm (the thickness of our fixed silver tissue samples). Assigning $Z$ as 5 nm (root mean square size of inhomogeneities in layer thickness) in the model best matched our reflectance measurements of the tissue and seems reasonable because the interfaces of the cells with the extracellular matrix are relatively smooth. Values of refractive index were chosen based on previous research [5,16] as 1.56 for cells densely filled with protein and 1.33 for the extracellular space around them. Noisy coherent reflections were made more realistic by averaging modelled spectra over 50 separate calculations.

The statistical variations in layer thicknesses of the cells (high refractive index) and the extracellular matrix (low refractive index) of the composite silver tissue were separately determined by analysing TEM images of the reflector stacks. These images were scaled to binary contrast and noise was reduced using a median filter with a 3 × 3 pixel range. Matlab code was written to measure the number of black and white pixels comprising regions of high- and low-refractive index of the tissue along many vertical lines in the adjusted TEM images (figure 3*a*). After the pixel counts were scaled to thicknesses in nanometre, the program then compiled the resulting histogram (figure 3*b*) and the skewed histograms were fit to gamma probability density functions with parameters $a$ and $b$ defined by the equation:

$$f(x; a,b) = x^{a-1}\frac{e^{-x/b}}{\Gamma(a)b^a}.$$

This distribution was found to have the best fit to the data when compared with other distribution

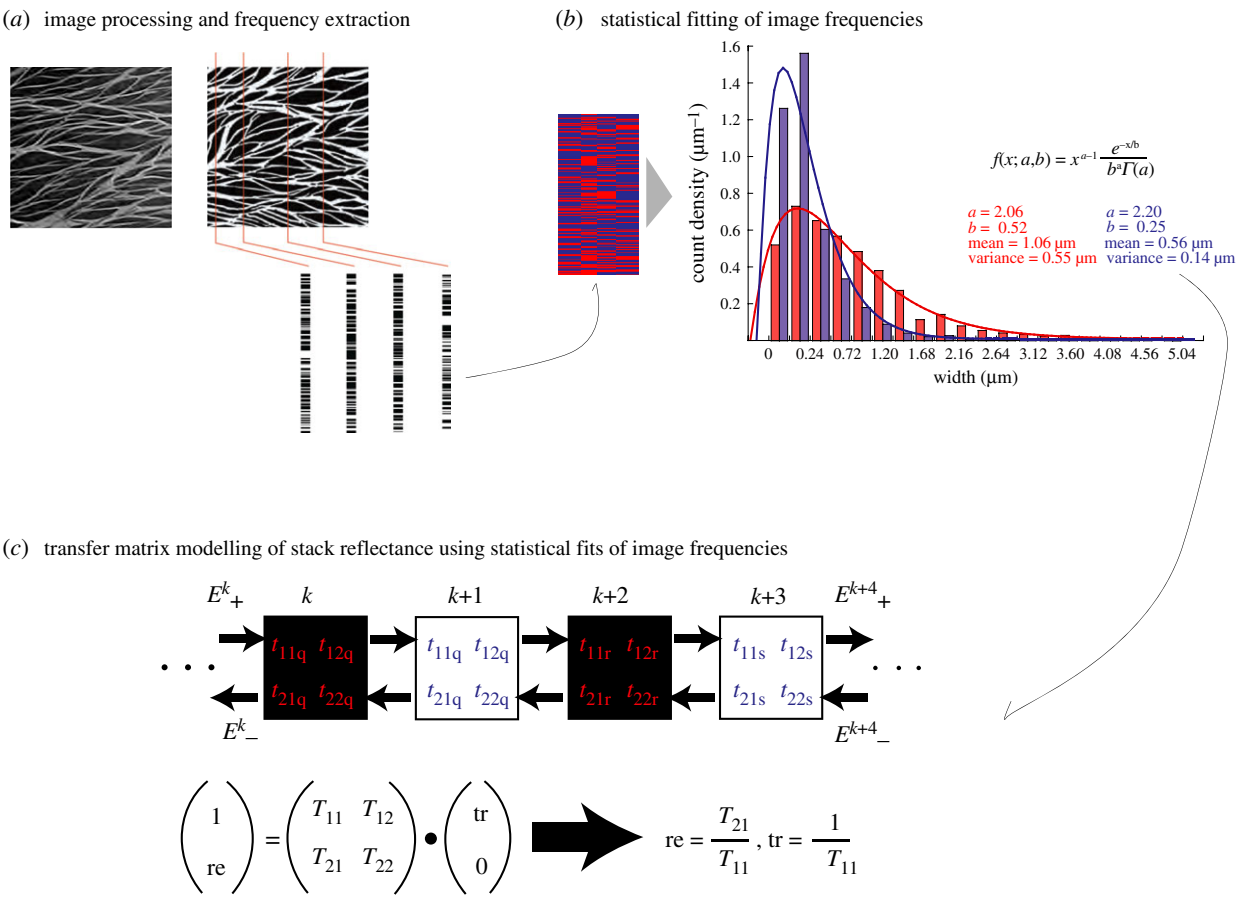


Figure 3. (*a*) TEMs were converted to binary images, and then converted to one-dimensional spatial components based on vertical transects through the image, simulating a normal angle of incident light. (*b*) The spatial components obtained from these vertical transects were then pooled [represented by the red ($n_h$) and blue boxes ($n_l$)], and their resulting spatial distributions fit to two different gamma distributions—one for high index regions, and the other for low index regions—as shown by the red and blue bars. The fit components of the gamma distributions are also shown in this panel. (*c*) Thicknesses were chosen from a gamma distribution as generated in (*b*), and input into a transfer-matrix model of reflectance. High- and low-index layers alternated and were chosen with frequencies dictated by the respective gamma-fit distributions. This panel shows a schematic of mathematics involved in the transfer-matrix method, with $k$ representing the layer being modelled, $t$ representing the components of the transfer matrices and $E$ represents the electric field at each interface.

functions typically used to fit skewed histograms such as normal, lognormal, logistic, log-logistic, Weibull and Birnbaum–Saunders. For gamma distributions, the mean is mathematically defined as $a \times b$ and the variance as $a \times b^2$. The parameters $a$ and $b$ resulting from TEM image analysis were then used to generate distributions of high- and low-refractive index layer thicknesses. Random choices of high and low thicknesses from these distributions were then used for the reflectance modelling.

To examine the effect a changing tissue transect angle has on reflectance, and thereby study the way in which reflectance from the silver tissue might change as the animal changes orientation, TEM images were rotated clockwise from 0° to 90° and the same vertical transects were drawn in each rotated image. For these models, incident light was always maintained at an incoming angle of 0° to the unrotated tissue and therefore always perpendicular to the new set of layer thicknesses (figure 4). New histograms were calculated as a function of image rotation and the resulting values, $a$ and $b$, were input into the modelling program. To further investigate our inferences about the biological structure's optical design, structural models were created in Adobe Illustrator using rectangles and a geometrical football shape called a vesica piscis to graphically represent the spindle-shaped cells. The shapes were then systematically varied in size and orientation (rotated from −25° to 25°) and subjected to the same analysis as the TEM images.

## 3. RESULTS

### 3.1. Light microscopy

The silver eye tissue comprises long, flat, thin, featureless cells (figures 5 and 6). Cell maximum widths and maximum thicknesses were relatively consistent at around 5 and 1 μm, respectively, but cell length varied greatly, from around 5 to 100 μm (averaging at approx. 60 μm). Under DIC illumination (figure 5*a*,*b*), these cells were featureless, with no apparent nuclei or other large organelles. Phase illumination of the cells produced a large, bright phase halo (figure 5*c*), suggesting that the cells had a high average refractive index, and no subcellular structures could be visualized even at high magnifications. DAPI staining and

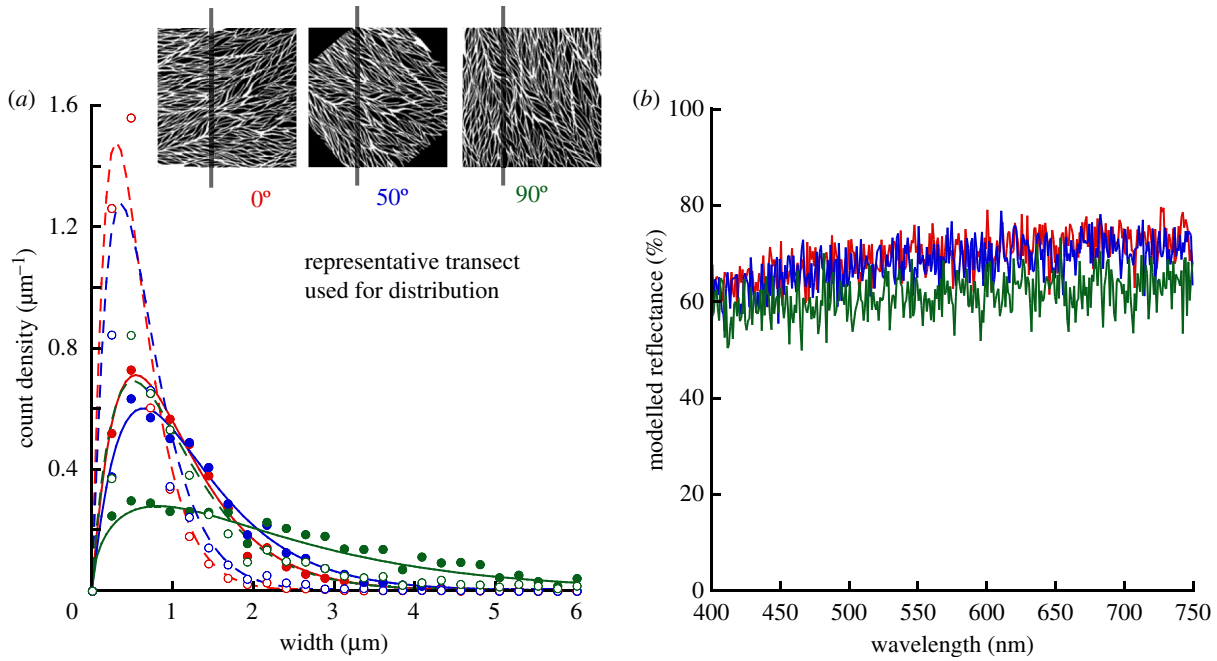


Figure 4. Effect of rotating the viewing angle in a horizontal plane around the animal. (*a*) Progression of histograms resulting from rotation of the TEM image with constant normal illumination. Filled red circles, 0° $n_h$; filled blue circles, 50° $n_h$; filled green circles, 90° $n_h$; open red circles, 0° $n_l$; open blue circles, 50° $n_l$; open green circles, 90° $n_l$. (*b*) The resulting static modelled reflectance data are constant with rotation of the structure under a constant illumination, showing that as a predator rotates around a squid, the eye will remain hidden. Red line, 0°; blue line, 50°; green line, 90°.

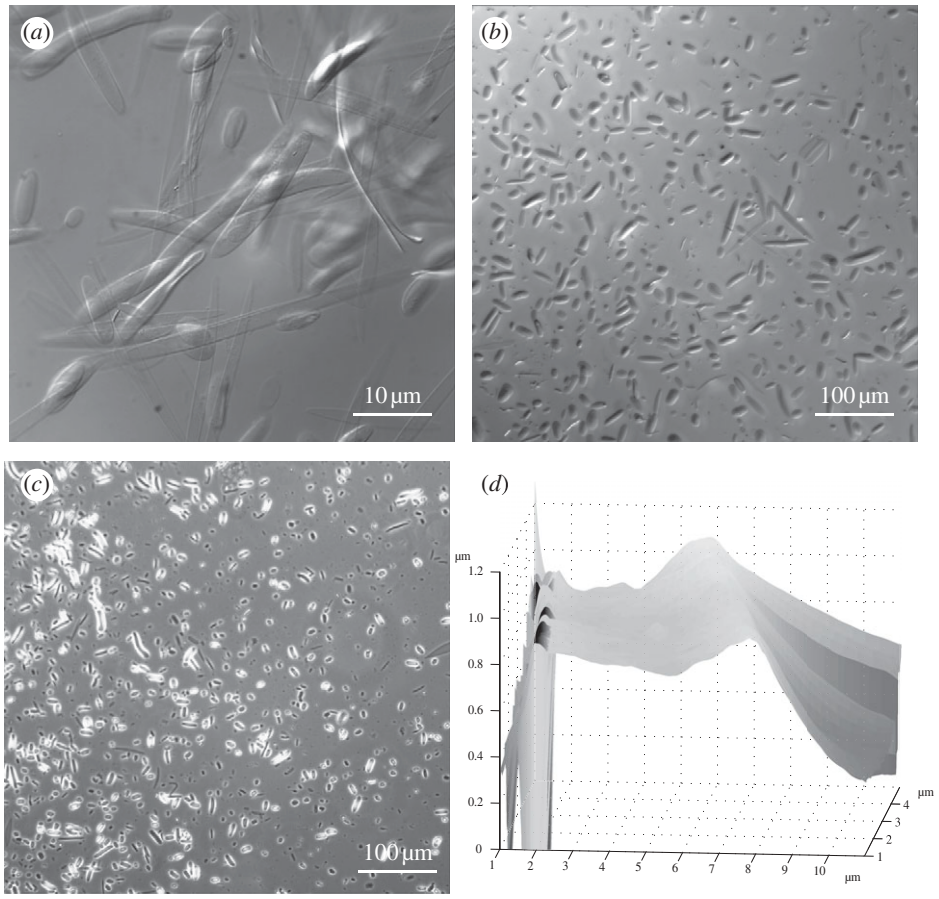


Figure 5. (*a*) 1000× DIC-illuminated light micrograph of silver tissue showing the spindle-shaped cells that comprise the silver tissue delaminated on a slide. Notice that the spindle-shaped cells are completely featureless and appear to lack nuclei in this view. (*b*) 100× DIC-illuminated light micrograph showing length distribution of the spindle-shaped cells. (*c*) 100× phase contrast illumination showing a bright phase halo around each spindle-shaped cell, indicating high refractive index. (*d*) Three-dimensional height profile of a single cell obtained by AFM.

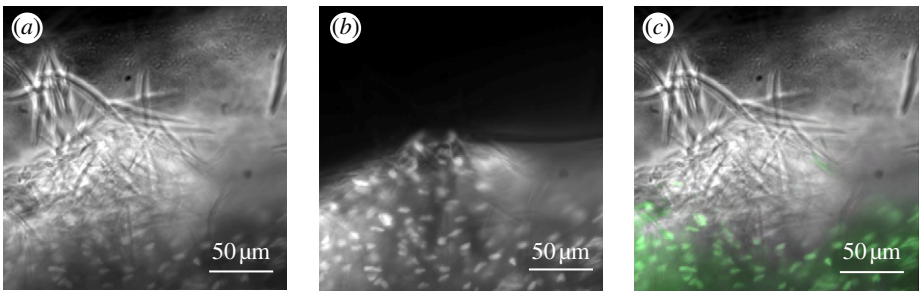


Figure 6. DAPI staining of silver tissue cells. (*a*) Dark field illumination; (*b*) DAPI fluorescence; (*c*) overlay of images (*a*,*b*). Nuclei are found interspersed throughout the tissue, but are located outside the spindle-shaped cells, and not inside them.

fluorescence microscopy of the tissue showed that while there were brightly staining nucleic acid-containing bodies in the tissue, they were all apparently extracellular (figure 6). These nucleic acid-rich masses were approximately 5 µm in diameter, suggesting the possibility that they may be nuclei extruded from the featureless, spindle-shaped cells.

### 3.2. Atomic force microscopy

AFM of unfixed tissue allowed us to measure the true physical thickness of the spindle-shaped structures in the absence of the optical artefacts introduced in light microscopy or the fixation artefacts introduced in TEM. AFM showed the maximum physical thickness of the spindle-shaped structures to be approximately 1.2 µm (figure 5*d*), consistent with the dimensions observed in TEM. Therefore, we did not consider possible tissue shrinkage owing to dehydration involved in processing tissue for TEM in our models.

### 3.3. Transmission electron microscopy

TEM of the tissue revealed packed, electron-dense spindle-shaped structures with an unstained region of relatively constant width separating them. The length of these spindle shapes observed in TEM was consistent with the cellular dimension perpendicular to the longest axis of the cells observed via light microscopy (figure 7*a*). Structures similar to this have been previously reported as 'platelets' in the eyelid of the *Loligo forbesi*, and a similar reflector was described lining one of the photophore types in the squid *Pterygioteuthis microlampas* [5,16]. The cells tended to be packed with the longest axis roughly parallel to the surface of the animal (see electronic supplementary material for a rendering of the three-dimensional packing of the cells). These micrographs showed that, consistent with their homogeneous appearance under DIC and phase illumination, the structures are uniformly filled with osmophilic, electron-dense material. These structures appeared to be bounded by a cell membrane, consistent with them being cells or packets of former cells (figure 7*b*).

Dispersed throughout the tissue, in between the densely staining spindle-shaped structures, were roughly spheroidal structures (figure 7*c*) consistent with the DAPI-stained material observed in fluorescence microscopy (figure 6) and consistent with the cell nuclei extruded from the spindle-shaped packets. To confirm that nuclei are exclusively located outside of the transparent spindles in this tissue, further work with confocal microscopy would be required.

At the distal outer edges of the eye, there is a distinctly green rim where the silver tissue inserts into the cartilaginous support tissue of the eye. In TEM, this region of the eye revealed loosely ordered, densely staining platelets approximately 70 nm thick (figure 7*d*), reminiscent of the reflector structure found in the *Euprymna scolopes* light organ [17].

### 3.4. Reflectance spectroscopy and optical modelling

The measured specular reflectance in the visible wavelength regions is flat over incident angles 15°–30° with intensity that varies by 25 per cent (figure 8*a*). We modelled this effect using a one-dimensional transfer-matrix model incorporating randomly varying gamma-distributed layer thicknesses of high (mean = 1.06 µm, variance = 0.55 µm) and low (mean = 0.56 µm, variance = 0.14 µm) refractive index (figure 8*b*). Incorporating partial incoherence owing to scattering in the model results in an overall decrease in reflectance as well as a disproportionate decrease at shorter wavelengths. In the modelled spectra, the per cent reflectance of the structure is primarily dependent on the number of cells stacked together—a value which is determined by the thickness of the tissue, as well as the angle of incidence of incoming light. In accordance with the reflectance measurements of the tissue, the shape of the broadband reflectance in our model of specular reflectance is independent of the angle of incidence up to 85° (data from 40° to 85° not shown) while the intensity varies little from 0° to 40° (figure 8*b*). The dependence of the modelled spectra with wavelength is comparable with the measured spectra. This portion of the modelling and measurement represents a viewer and illuminant both rotating at equal angles from the normal (as defined by specular reflection) in the lateral plane around the animal.

To explore the geometrical differences between a two-dimensional stack of these spindle shapes from a stack of infinite planes, we compared the layer thickness distributions from rotated transects of a stack of parallel planes with those of the TEM images of the packed cells. The means and variances of fitted gamma distributions of these two images begin to depart significantly at approximately 50°. Thus, while our

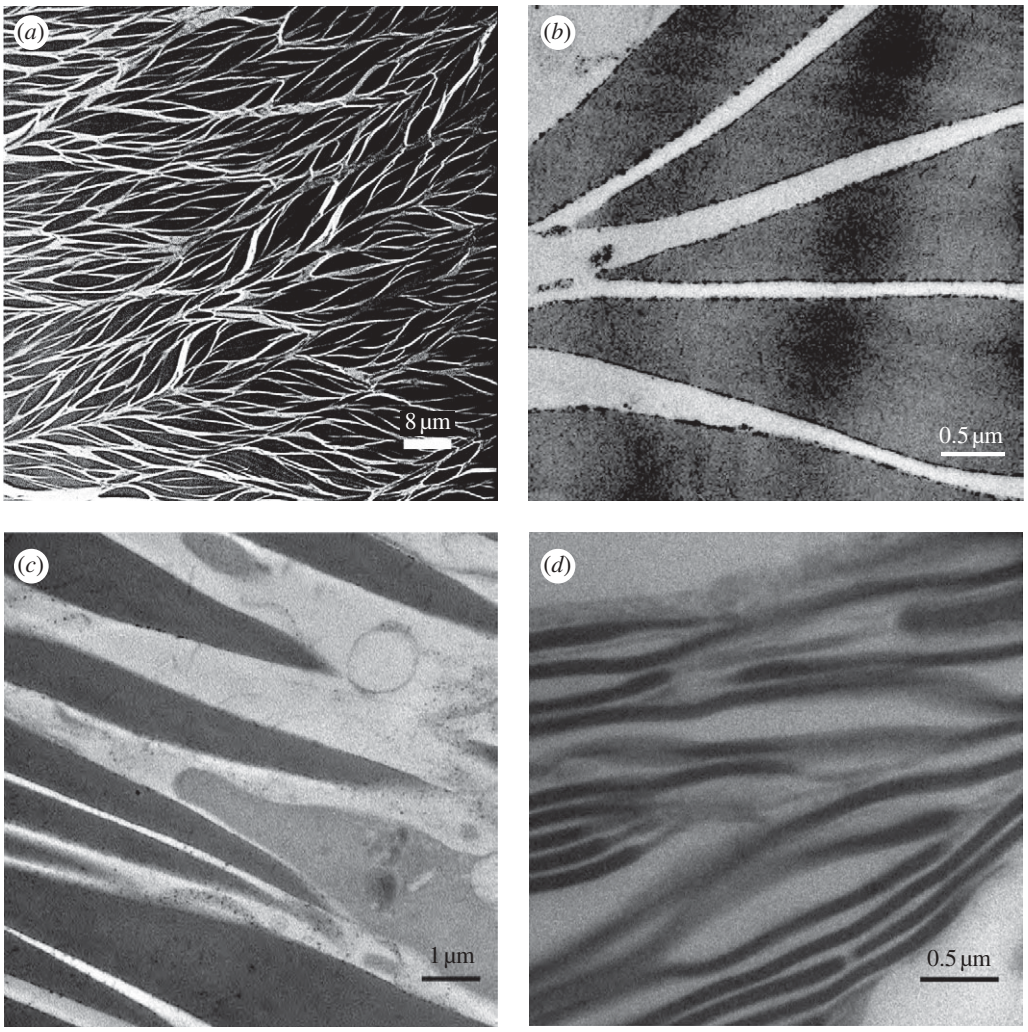


Figure 7. TEM micrographs of silver eye tissue. (*a*) TEM micrograph of silver eye tissue showing the large areas of homogeneously packed featureless spindle-shaped cells that characterize the tissue. (*b*) High magnification view showing osmium granules precipitated on cell membranes. (*c*) A nucleus located outside of the spindle-shaped cells. The lower staining density suggests that the nucleus may have a lower refractive index than the densely packed protein in the interior of the spindle-shaped cells. (*d*) Platelets in the green outer rim of the eye, suggesting a role as a precursor to template the homogeneous fill of the spindle cells.

use of the transfer matrix model is an appropriate probe into the optical properties of this complex tissue, the structure in the second and third dimensions may also be important to the eye covering's optical functions. TEM images of the packed spindle structures, such as in figure 7*a*, show a slight anisotropy in spindle positioning between the vertical and horizontal directions. We used the observation to gain additional insights regarding the sensitivity of the reflectance spectra to changes in the distributions of layer thicknesses that a fixed illuminant would produce with a rotation of the two-dimensional structure. We chose the new thickness distributions calculated with rotated transects to approximate the effect of a viewer moving in a circle in the lateral plane around the animal while illumination remains constant. While rotating the TEM image from 0° to 90° resulted in a broadening and flattening of the distribution densities of the thicknesses of high- and low-refractive index (figure 4), the modelled reflectance spectra in the visible wavelength region remains relatively unaltered (figure 4). The slight decrease in intensity with image rotation in the model is a result of the decrease in the number of cells that fit into the fixed tissue thickness owing to the preferred stacking of the anisotropic spindle shapes parallel to the surface plane. Changes in reflectance with incident angle for each transect were also calculated (data not shown) and showed the same relative dependence in intensity and shape as the 0° transect.

To examine the effects of shape, size and packing of cells on thickness distributions and the resultant optical properties of a structure, we explored how systematically varying arrangements of specific shapes (either rectangles or the vesica piscis) affect the thickness distributions (or histograms) of high- and low-refractive index when these shapes are of a similar size scale to that observed in the silver tissue (figure 9). A vesica piscis is a rounded shape with pointed ends formed by the intersection of two circles, and is the closest simple geometric approximation to the spindle-shaped cross sections of the cells observed in the silver tissue. We compared the histograms of thicknesses of high- and low-refractive

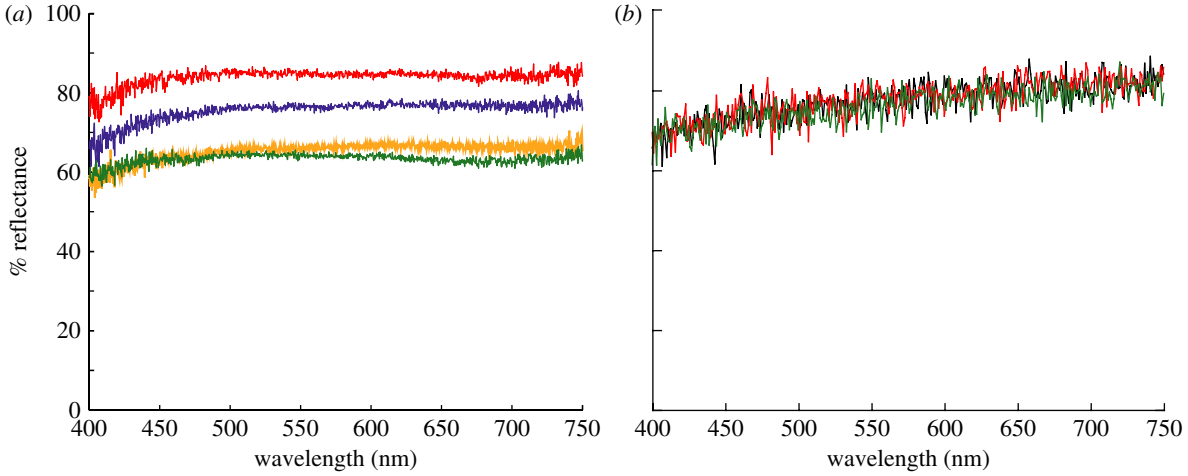


Figure 8. Measured and modelled angle dependence of silver tissue reflectance. (*a*) Measured reflectance from the silver eye tissue of *L. opalescens* at several angles of normal incidence using the instrument schematized in figure 2. Red line, 15°; blue line, 20°; yellow line, 25°; green line, 30°. (*b*) Modelled reflectance of the silver tissue with changing angle of incidence generated using the method shown in figure 3. Black line, 0°; red line, 15°; green line, 30°.

indexes for differently packed shapes to the TEM images. For simple quantification of these effects on spectra, we compared both the averaged modelled reflectance at visible wavelengths and the resultant standard deviation of this reflectance. In this comparison, higher standard deviations represent greater variations in reflectance with wavelength; thus, periodically ordered shapes will have higher standard deviations.

The ordered packing of rectangles of a single size results in a sharply peaked histogram distribution (in both high- and low-refractive indexes) typical of a classical Bragg stack, while the ordered packing of vesicae piscis of single size results in gamma-distributed low-refractive index regions [figure 9*a*(i)]. Arranging the vesicae piscis periodically results in a high-refractive index layer thickness distribution that almost linearly increases and peaks at the maximum width of the chosen vesica piscis and then drops to zero (figure 9*a*(ii)). Introducing rotation and variations in size to the packed vesica piscis shapes contributes several lower density peaks to the histograms at greater length scales, corresponding to the new layer thicknesses encountered. This permits a gradual decline in height and an increase in length of the tail of the distributions while decreasing the maximum density, resulting in a close match with the thickness distributions of the biological structure [figure 9*a*(iii–v)]. The modelled reflectance spectra from these structures demonstrate that simply changing the shape from a rectangle to a vesica piscis of the same size significantly increases the intensity of reflectance in the visible and reduces the standard deviation of the reflectance with wavelength. Simply rotating the rectangle shape produces gamma-distributed thicknesses for the low refractive index but results in lower reflectances owing to lower packing densities (data not shown). This shows that the spindle shape increases the density of non-ordered packing allowing for increased reflectance in a given tissue thickness, and also allows for smoother variations in layer thickness distributions, contributing to broadband reflectance. Furthermore, packing random orientations of rotated vesicae piscis further broadens the distribution of layer thicknesses and increases the reflectance to a level comparable with that modelled from the actual TEM image (figure 9*b*). Therefore, the shape of the cells alone is responsible for most of the relatively high reflectance and broadband characteristics of the silver tissue, while more efficient (i.e. higher density) packing results from the presence of spindles of different sizes and rotations, increasing the reflectance and broadening the layer thickness distributions. The variation in cell length and the long-axis orientation and packing also contributes to the variation in spindle size and rotation observed in the two-dimensional TEM transects.

### 3.5. Protein composition

The silver tissue covering the squid eyes is primarily composed of relatively small but abundant proteins, reminiscent of the crystallin protein composition of lens cells. In the silver tissue, these proteins are of low molecular mass, ranging from 21 to 37 kD, yielding six bands as resolved by one-dimensional SDS–PAGE (figure 10*a*). The apparent molecular masses of the six bands are 21, 24, 26, 29, 34 and 37 kD; together, they constitute 75 per cent of the total protein content of the tissue.

### 3.6. Western blotting and amino acid composition

Five of the six abundant small molecular mass fractions of the silver tissue total protein composition (21, 24, 29, 34 and 37 kD) showed positive reflectin immunoreactivity. However, the most abundant protein constituent of the pool with a molecular mass of 26 kD and representing 24 per cent of the total protein mass in the tissue, did not react with the reflectin antibody (figure 10*b*,*c*).

The reflectin immunopositive proteins from the silver eye tissue had the unusual amino acid composition found in the reflectins expressed in the dermal

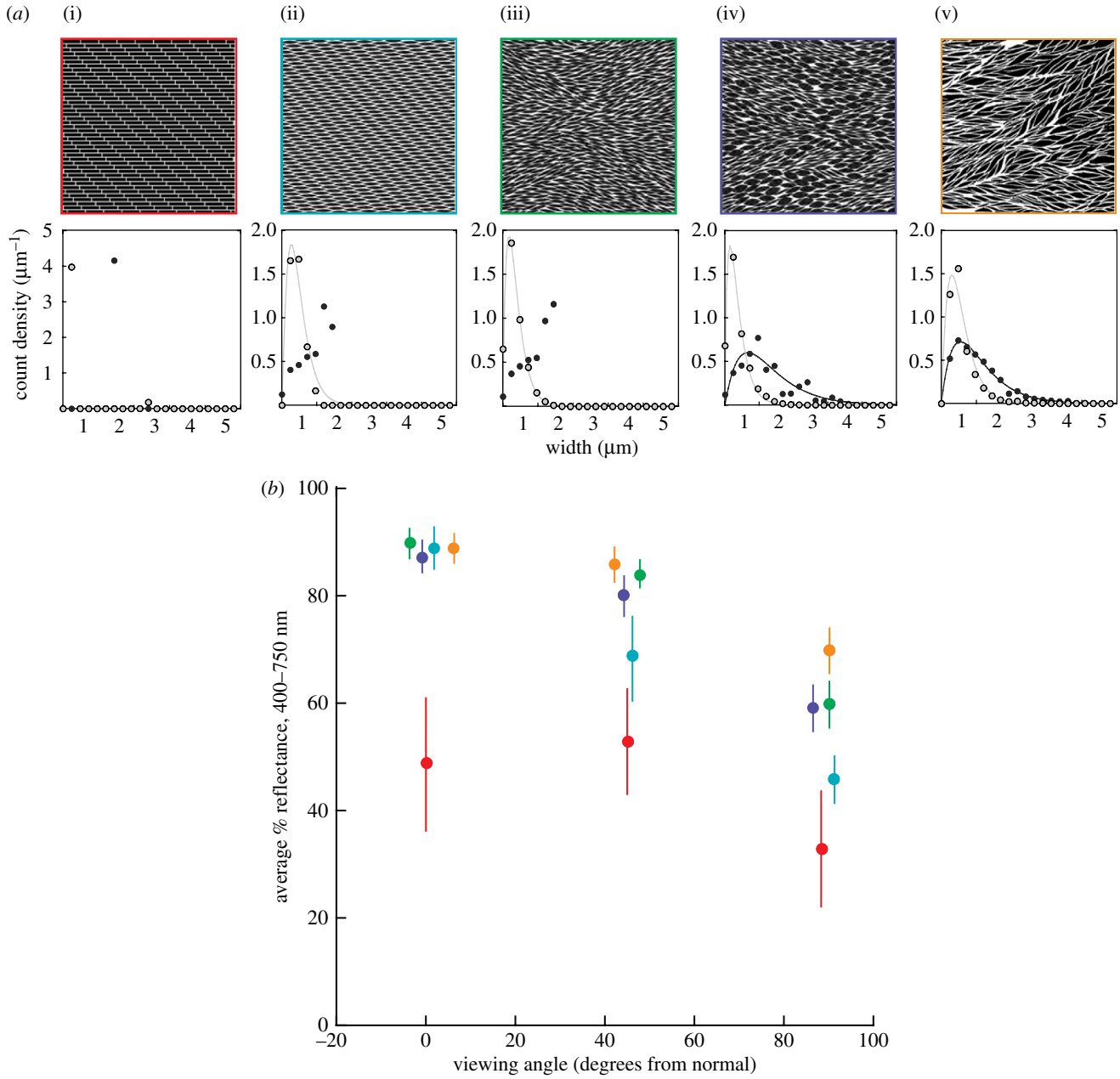


Figure 9. (*a*) Schematic designs to replicate aspects of TEM data and their respective histograms. (i–v) We tested aligned rectangle shapes; small, uniform vesica piscis shapes; uniform vesica piscis shapes rotated between −25° and 25°; four different sizes of vesica piscis rotated between −25° and 25° in 5° intervals and randomly assembled. Bottom row shows the corresponding histograms, with replication of the silver tissue improving from (i–v). Light circles represent layers with low index and dark circles represent layers with high refractive index. (*b*) Average per cent reflectance from 400 to 750 nm (dots) and standard deviation (bars) for each corresponding design above. The dots and bars are colour-coded by the designs above. Each addition of complexity to the model improved its replication of the broadband, high reflectance observed in the squid silver tissue.

iridophores of the squid [11], characterized by high percentages of methionine, arginine and tyrosine, and a near absence of small hydrophobic residues. The proteins identified in the silver tissue were composed of 16–19% methionine, 7–8% arginine and 16–20% tyrosine, and had near-undetectable levels of the hydrophobic amino acids leucine, isoleucine and valine. In contrast, the reflectin-immunonegative proteins in the silver tissue had a nearly inverse amino acid composition: they were composed of less than 2 per cent each of arginine, methionine and tyrosine, while being enriched in alanine, isoleucine and leucine. These reflectin-immunonegative proteins had an alanine content of 20 per cent, isoleucine content of 17 per cent and leucine content of 15 per cent.

## 4. DISCUSSION

The silvery reflective tissue surrounding the eyes of squid in the family Loliginidae appears to have several novel optical features contributing to camouflage from lateral-looking predators in shallow and midwater pelagic environments (species depth distribution approx. 0–300 m). The optical properties of the tissue are in agreement with the idealized case predicted for camouflage in this environment (figure 11) [18] and

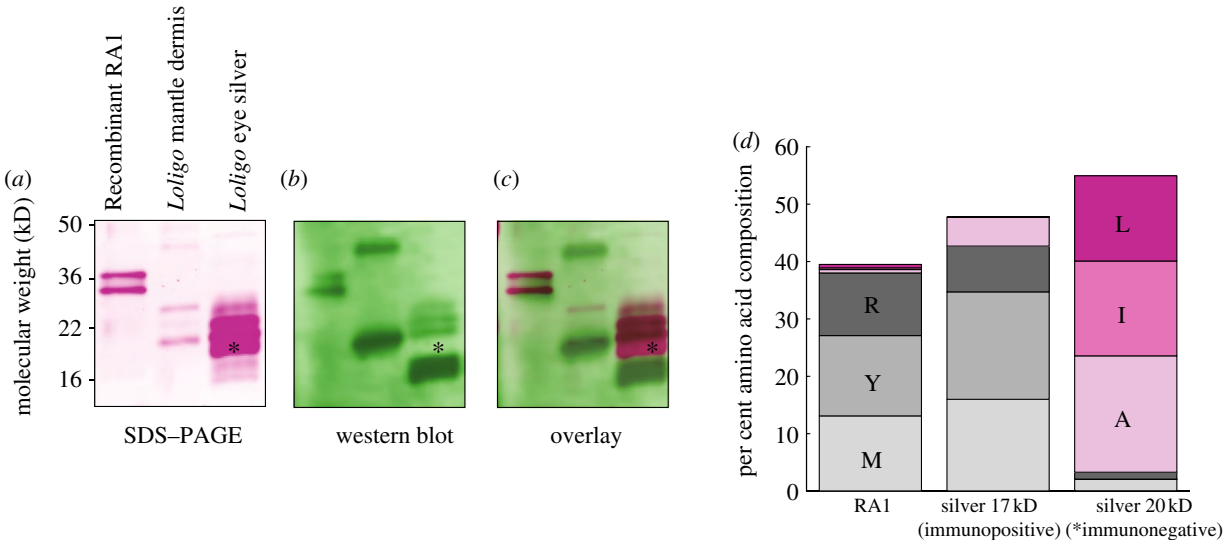


Figure 10. Western blot and amino acid composition of silver eye tissue. Asterisks indicate the location in each blot of the most highly abundant, reflectin-immunonegative protein in the silver eye tissue. (*a*) SDS–PAGE of recombinant reflectin RA1, total *L. opalescens* mantle dermis and total *L. opalescens* silver eye covering. (*b*) Western blot using an antibody against recombinant reflectin A1 shows the presence of reflectins present in several of the abundant protein species in the silver tissue. (*c*) An overlay of the SDS–PAGE and Western blot shows that the most abundant protein species in the silver tissue does not cross-react with the reflectin antibody. (*d*) Amino acid composition of reflectin A1, a reflectin cross-reactive fraction of the silver tissue and the immunonegative major protein band from the silver tissue. The non-reactive major protein component of the silver tissue has a radically different protein composition from the reflectin-immunopositive proteins, suggesting that it may play an intracellular role in spindle assembly.

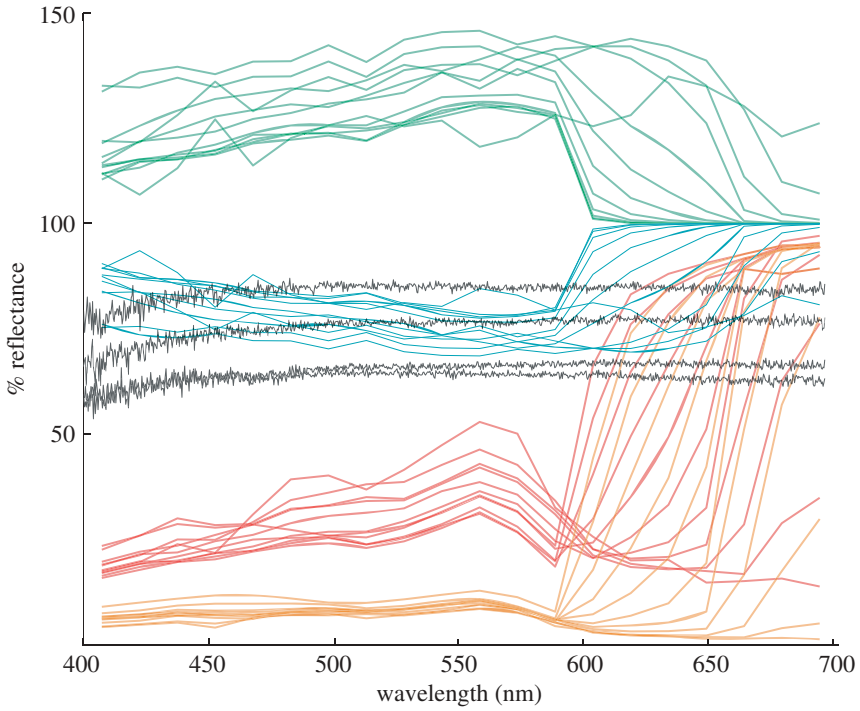


Figure 11. Angle-dependent reflectance of *L. opalescens* in context with the optimal reflectances for underwater camouflage at different depths (every 5 m between the surface and 50 m) and viewing angles. Black traces reproduce the data shown in figure 7 for angle-dependent reflectance of *L. opalescens* silver eye tissue. Green traces are the optimal specular reflectances looking towards the sun, and blue traces are optimal specular reflectances looking away from the sun. Red traces are optimal reflectance for a diffuse reflector with the viewer looking into the sun, and orange traces are optimal reflectance for a diffuse reflector with the viewer looking away from the sun solid black traces, Loligo eye reflectance (15°, 20°, 25° and 30°). The *L. opalescens* reflectances appear to replicate a hybrid between the specular and diffuse solutions quite well, consistent with our observation that the reflector is largely specular but with some diffuse components.

involve specularly reflecting dielectric stacks for camouflage in a dynamic midwater environment in which the biological constraint for limited tissue thicknesses prevent efficient diffuse scattering.

Johnsen & Sosik [18] describe ideal scattering for matching a cylindrical light field in a pelagic environment for both an ideal mirror and an ideal Lambertian scatterer at different depths and angles. The squid silver structure, with its slightly curved Bragg stacks, primarily appears to exhibit specular reflectance with some diffuse scattering. Placed in the context of the modelled radiance from the work of Johnsen & Sosik [18], the reflectances of the squid silver tissue that we measured is a good average of the solutions to camouflage in the top 50 m of open water (figure 11). The 84 per cent average reflectance across all wavelengths produced by the tissue of the squid eye appears to represent a good compromise strategy between the optimal reflectance at the surface and at 50 m depth, which overlaps with the depth distribution of loliginids [19]. According to the Johnsen & Sosik model, the ideal case of camouflage in the top 200 m of the open ocean requires a nearly flat average reflectance in the visible up to about 605 nm. Our transfer matrix model predicts a nearly flat reflectance from this tissue throughout the entire visible region with an intensity that drops with raking incident angles, and this modelled result agrees well with the measured specular reflectance. We modelled the slight decrease in reflectance at lower wavelengths (approx. 400 nm) in the measured reflectance spectra by considering that the light is partially incoherently scattered by variations of 5 nm (r.m.s. value) from a perfectly flat interface. This degree of incoherence is consistent with the fairly smooth surfaces viewed using TEM and AFM. Both the measured and modelled silver reflectance depart from the predicted optimum most conspicuously in the 650 nm region of the visible spectrum, where Raman scattering makes red light nearly isotropic and increased in intensity relative to blue light at depth [20], suggesting that the silver tissue could improve its camouflaging ability by modulating its reflectance in the red region of the spectrum—fascinatingly, the dynamic iridophores of the *L. opalescens* dermis do exactly this [11,21].

The structure we have characterized exhibits components of both diffuse and specular reflectances and may capitalize on different features of these reflectors in the environment in which it evolved. An ideal vertical camouflaging structure for the eye should not change its reflectance with viewing angle (with regards to the reflectance a predator sees with changing position), as the retina of the eye should be hidden from all observation angles and from a moving predator. Typically, in the case of complete specular reflection from a dielectric stack, reflectance changes with observation angle in both colour and intensity. In the context of underwater camouflage, these changes in specular reflection would be conspicuous for example, when sunlight changes relative direction. The characteristics of the squid's optical structure may help to reduce angular dependence owing to specularity for two reasons. First, while the spindle shape of the cells provides the requisite distribution of layers with high- and low-refractive indexes to provide broadband reflectance, it may also contribute to diffuse scattering owing to non-parallel interfaces. Second, the fact that the optical layer has a distinct (but not symmetric) three-dimensional morphology (because the spindle-shaped cells have a high aspect ratio in both perpendicular directions) may also contribute to some angle independence of the optical response [22]. We measured the angle dependence of specular reflection from the eye using a goniometer and showed it to be low (figure 8*a*). While further measurements are required to determine the full scattering profile of this optical structure, here we illustrate the potential optical advantages of this three-dimensional system by modelling both the specular angle dependence of a stack with randomized, gamma-distributed layer thicknesses (figure 8*b*) and by modelling the reflectance from the rotated structure (figure 4). This modelled extraction of the two-dimensional structure helps support the concept that morphology contributes to angle independence by illustrating that a viewer moving in a horizontal plane around the eye probably sees the same reflectance from any angle.

The spindle shape of the cells also directly contributes to cell packing and therefore simultaneously to high reflectance and to the distribution of layer thicknesses contributing to flat reflectance. To probe these relationships, we explored the effects of shape type, shape size and shape orientation on our model of reflectance and demonstrated that the observed structure achieves necessary layer thickness distributions for flat, high visible reflectance with few geometric parameters. The thicknesses of the layers with low refractive index become gamma-distributed simply by changing the geometry of the shape from a rectangle to a vesica piscis. The thicknesses of layers with high refractive index observed in the squid silver structure have a more complex dependence on spindle sizes and rotation (figure 9). Introducing size variation to an equal number of these shapes results in noisy gamma-distributed layer thicknesses while rotating the shapes helps smooth the tail of the distribution. Our simulation using vesicae piscis of four sizes and 11 orientations comes close to replicating the experimentally observed distribution of high and low refractive indexes. However, the modelled reflectance data are also matched by a simpler model that considers rotation of singly sized vesicae piscis. Analysis of these models shows that the details of the biological structure provide the closest match to the ideal camouflaging reflectance.

Another attractive feature of this structure is the ease with which one geometrical element—the spindle—can be mimicked and efficiently packed. The packing of spindle-shaped cells in the silver tissue appears related to studies that show randomly packed ellipsoids (axis ratio—0.8 : 1 : 1.25) exhibit large packing densities, only second to cubes, when compared with cylinders, tetrahedrons, cones and spheres [23,24]. An additional required element of this structure is the maintenance of the low-index space between the high-index spindles, which is as important to the optical function as the high-index spindle shapes, although loose packing of these shapes will result in some

amount of low-index space in the structure. We speculate that the regular thicknesses of the intercellular spaces observed in our images may be owing to an extended extracellular matrix, which we observed collapsed in some of our TEM images (data not shown).

Extruding nuclei from the spindle cells seems necessary for the observed optical function of the tissue, as this optimizes the optical homogeneity of the spindle-shaped cells. With nuclei inside the spindle shapes, depending on their position within the cell, spatial structure with frequencies on the order of visible wavelengths could be added, possibly introducing coloured reflectance to the tissue. Extruded from the cells, each nucleus can function optically as its own high-index element, thereby contributing to maintain the thickness distribution necessary for perfectly flat reflectance in the visible (figure 5). Nuclear extrusion for an optical function also occurs in lens cells of both squids and humans, where, if the nuclei were present, lenses would be nearly opaque owing to scattering [25,26].

The protein composition of the tissue and our observations of the possible precursor structures suggest a hypothesis about its self-assembly from living cells. Achieving a perfectly homogeneous, high-index, non-scattering infill of protein is a non-trivial process as high concentrations of similar proteins usually cause aggregation, plaque formation and associated light scattering [27]. The somewhat disorganized platelets present in the outer green rim of the eye (figure 7*d*) are reminiscent of similar structures observed in the *L. opalescens* dermal iridophores and the light organ reflector of *Euprymna scolopes*. These reflective platelets are largely composed of canonical reflectin proteins, characterized previously (data not shown) [17,11]. We hypothesize that in the silver tissue, approximately 70 nm platelets composed of canonical reflectins could form a template of aromatic residues that would be both water- and lipid-soluble, facilitating subsequent homogeneous infill of the cells with the novel, hydrophobic protein shown in figure 10. In this model of spindle cell development, as the infill occurs, the nucleus is extruded and the cell becomes quiescent, resulting in the optically homogeneous spindles with external nuclei that we observed with TEM. This possible mechanism for achieving relatively large, optically homogeneous structures, combined with the elegant packing of the spindle shapes to achieve useful optical properties presents intriguing possibilities for technological mimicry and innovation.

This research was supported by the Office of Naval Research through grant no. N00014-09-1-1053 to Duke University via subaward no. 09-ONR-1115 and (for support of D.E.M.) by the Army Research Office grant no. W911NF-10-1-0139.

## REFERENCES

1 Yoo, K. M. & Alfano, R. R. 1989 Broad bandwidth mirror with random layer thicknesses. *Appl. Opt.* **28**, 2456–2458. (doi:10.1364/AO.28.002456)
2 McKenzie, D. R., Yin, Y. & McFall, W. D. 1995 Silvery fish skin as an example of a chaotic reflector. *Proc. R. Soc. Lond. A* **451**, 579–584. (doi:10.1098/rspa.1995.0144)
3 Parker, A. R., McKenzie, D. R. & Large, M. C. 1998 Multilayer reflectors in animals using green and gold beetles as contrasting examples. *J. Exp. Biol.* **201**, 1307–1313.
4 Vukusic, P., Kelly, P. & Hooper, I. 2009 A biological submicron thickness optical broadband reflector characterized using both light and microwaves. *J. R. Soc. Int.* **6**, S193–S201.
5 Denton, E. J. & Land, M. F. 1971 Mechanism of reflexion in silvery layers of fish and cephalopods. *Proc. R. Soc. Lond. B* **178**, 43–61. (doi:10.1098/rspb.1971.0051)
6 Menter, D. G., Obika, M., Tchen, T. T. & Taylor, J. D. 1979 Leucophores and iridophores of *Fundulus heteroclitus*: biophysical and ultrastructural properties. *J. Morph.* **160**, 103–120. (doi:10.1002/jmor.1051600107)
7 Pavesi, L. & Dubos, P. 1997 Random porous silicon multilayers: application to distributed Bragg reflectors and interferential Fabry–Pérot filters. *Semicond. Sci. Technol.* **12**, 570. (doi:10.1088/0268-1242/12/5/009)
8 Ding, T., Song, K., Clays, K. & Tung, H. 2009 Fabrication of 3D photonic crystals of ellipsoids: convective self-assembly in magnetic field. *Adv. Mat.* **21**, 1936–1940. (doi:10.1002/adma.200803564)
9 Sweeney, A. M., Des Marais, D. L., Ban, Y. A. & Johnsen, S. 2007 Evolution of graded refractive index in squid lenses. *J. R. Soc.* **4**, 685–698. (doi:10.1098/rsif.2006.0210)
10 Tomorev, S. I. & Zinovieva, R. D. 1988 Squid major lens polypeptides are homologous to glutathione S-transferase subunits. *Nature* **336**, 86–88. (doi:10.1038/336086a0)
11 Izumi, M. *et al.* 2010 Changes in reflectin protein phosphorylation are associated with dynamic iridescence in squid. *J. R. Soc. Interface* **7**, 549–560. (doi:10.1098/rsif.2009.0299)
12 Vasicek, A. 1960 *Optics of thin films*, pp. 254–261. Amsterdam, The Netherlands: North-Holland.
13 Katsidis, C. C. & Siapkas, D. I. 2002 General transfer-matrix method for optical multilayer systems with coherent, partially coherent, and incoherent interference. *Appl. Opt.* **41**, 3978–3987. (doi:10.1364/AO.41.003978)
14 Mitsas, C. L. & Siapkas, D. I. 1995 Generalized matrix method for analysis of coherent and incoherent reflectance and transmittance of multilayer structures with rough surfaces, interfaces, and finite substrates. *Appl. Opt.* **94**, 1678–1683. (doi:10.1364/AO.34.001678)
15 Sutherland, R. L., Mathger, L., Hanlon, R. T., Urbas, A. M. & Stone, M. O. 2008 Cephalopod coloration model. I. Squid chromatophores and iridophores. *J. Opt. Soc. A* **25**, 588–2044. (doi:10.1364/JOSAA.25.000588)
16 Arnold, J. M., Young, R. E. & King, M. V. 1974 Ultrastructure of a cephalopod photophore. II. Iridophores as reflectors and transmitters. *Biol. Bull.* **147**, 522–534. (doi:10.2307/1540737)
17 Crookes, W. J., Ding, L., Huang, Q. L., Kimbell, J. R., Horwitz, J. & McFall-Ngai, M. J. 2004 Reflectins: the unusual proteins of squid reflective tissues. *Science* **303**, 235–238. (doi:10.1126/science.1091288)
18 Johnsen, S. & Sosik, H. M. 2003 Cryptic coloration and mirrored sides as camouflage strategies in near-surface pelagic habitats: implications for foraging and predator avoidance. *Limnol. Oceanogr.* **48**, 1277–1288. (doi:10.4319/lo.2003.48.3.1277)
19 Cargnelli, L. M., Griesbach, S. J., McBride, C., Zetlin, C. A. & Morse, W. W. 1999 NOAA Technical Memorandum NMFS-NE-146.

20 Stavn, R. H. & Wiedemann, A. D. 1988 Optical modeling of clear ocean light fields: Raman scattering effects. *Appl. Opt.* **27**, 4002–4011. (doi:10.1364/AO.27.004002)
21 Tao, A. R., DeMartini, D. G., Izumi, M., Sweeney, A. M., Holt, A. L. & Morse, D. E. 2010 The role of protein assembly in dynamically tunable bio-optical tissues. *Biomaterials* **31**, 793–801. (doi:10.1016/j.biomaterials.2009.10.038)
22 Mangaiyarkarasi, D., Breese, M. B. H. & Ow, Y. S. 2008 Fabrication of three dimensional porous silicon distributed Bragg reflectors. *Appl. Phys. Lett.* **93**, 221905. (doi:10.1063/1.3040304)
23 Li, S. X., Zhao, J., Lu, P. & Xie, Y. 2010 Maximum packing densities of basic 3D objects. *Chin. Sci. Bull.* **55**, 114–119. (doi:10.1007/s11434-009-0650-0)
24 Chaikin, P. M., Donev, A., Man, W., Stillinger, F. H. & Torquato, S. 2006 Some observations on the random packing of hard ellipsoids. *Ind. Eng. Chem. Res.* **45**, 6930–6965. (doi:10.1021/ie060032g)
25 Benedek, G. B. 1971 Theory of transparency of the eye. *Appl. Opt.* **10**, 459–473. (doi:10.1364/AO.10.000459)
26 West, J. A., Sivak, J. G. & Doughty, M. J. 1995 Microscopical evaluation of the crystalline lens of the squid (*Loligo opalescens*) during embryonic development. *Exp. Eye Res.* **60**, 19–35. (doi:10.1016/S0014-4835(05)80080-6)
27 Cromwell, M. E. M., Hilario, E. & Jacobson, F. 2006 Protein aggregation and bioprocessing. *AAPS J.* **8**, E572–E579. (doi:10.1208/aapsj080366)